# Evaluation of the $Ni_3Al$ Base Alloys IC221 and IC218LZr

E. Samuelsson, P. W. Keefe
Special Metals Corporation
New Hartford, NY

R. W. Furgason
Ladish Company
Cudahy, WI

## Abstract

$Ni_3Al$-base alloys are being considered for a range of applications, where their high strength at elevated temperatures can be utilized. This paper summarizes the results of physical metallurgy evaluations of IC221 and IC218LZr which are alloys suitable for commercial applications.

Ingot sizes of 406 mm and 102 mm diameter were evaluated. Initial solidification in alloy IC218LZr occurs by precipitation of $\gamma$ dendrites. The remaining liquid is enriched in alloying elements, and final solidification occurs by a $\gamma$-$\gamma'$ eutectic reaction, dominated by the $\gamma'$ phase. IC221, which has a higher Zr content, solidifies by the same sequence, except final solidification occurs by freezing of a zirconium-rich eutectic. Energy and wavelength dispersive x-ray analysis indicate that the precipitated zirconium phase is $Ni_7Zr_2$. The reason that $Ni_7Zr_2$ precipitates rather than $Ni_5Zr$, which would be expected for an alloy containing only 1.8 weight % Zr, is not fully understood. However, it is probable that the strong interaction between nickel and aluminum leads to a decreased activity of nickel in the interdendritic fluid.

Mechanical properties were evaluated at temperatures from 760°C to 1038°C. In this temperature range, the yield strength decreases with temperature and minimum ductility is at approximately 950°C. Comparative evaluation of compression yield strength indicates that IC221 is approximately 500 MPa stronger than IN718 in the temperature range of 760°C to 1038°C.

This project demonstrates that $Ni_3Al$ base alloys can be consumably remelted into production-size ingots without deleterious segregation or ingot cracking.

Superalloys 1992
Edited by S.D. Antolovich, R.W. Stusrud, R.A. MacKay,
D.L. Anton, T. Khan, R.D. Kissinger, D.L. Klarstrom
The Minerals, Metals & Materials Society, 1992

## Introduction

In recent years the interest in intermetallic alloys, including nickel aluminide alloys, has increased. Numerous articles deal with various aspects of nickel aluminides; some useful review articles are those by Stoloff[1], Pope[2], Sen[3] and Sikka[4]. Sikka[5] has also discussed the commercialization of nickel aluminide alloys that were developed by Oak Ridge National Laboratory (ORNL).

This paper deals with properties of the two $Ni_3Al$ base alloys, IC218LZr and IC221 whose compositions are given in Table I. These alloys have similar compositions except for the higher content of zirconium in IC221. IC218LZr is intended for wrought applications, while IC221 is intended for cast applications. Only as-cast structures and properties of the alloys are evaluated in this study.

The alloy samples evaluated were produced by vacuum induction melting (VIM) followed by consumable electrode remelting. Samples from 102 mm diameter ingots of both alloys were evaluated, as were samples from a 406 mm diameter ingot of IC221. The 406 mm IC221 ingot is believed to be the largest sound, consumable-electrode-remelted ingot produced. The macrostructure of it is shown in Figure 1.

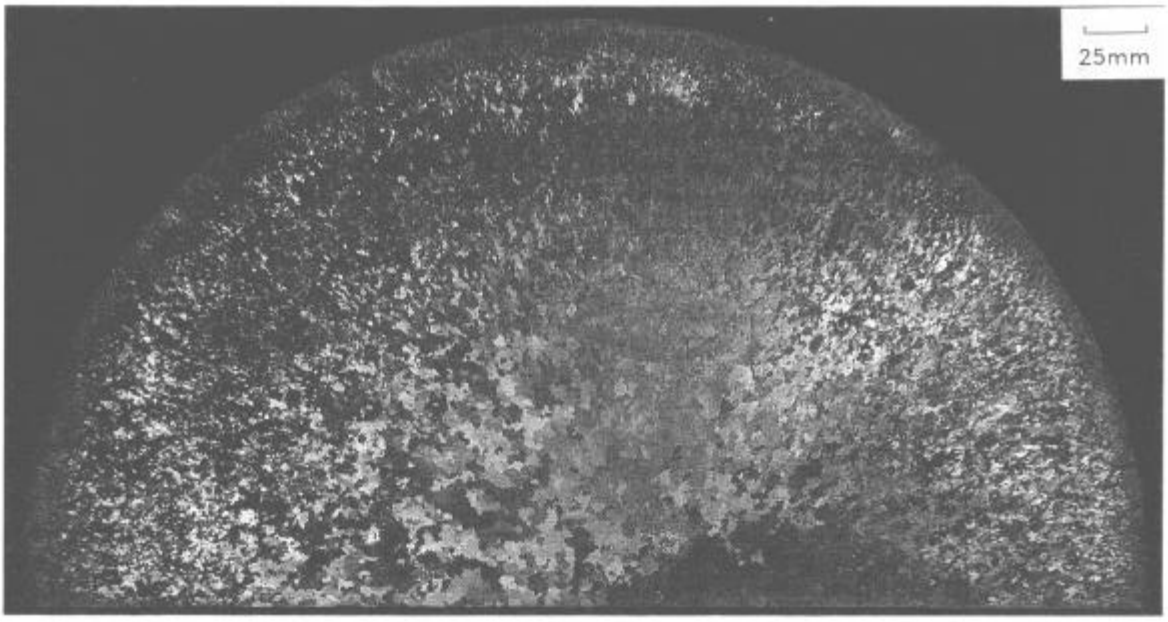


**Figure 1** Macrostructure of 406 mm diameter IC221 ingot. Canada etch.

## Solidification Sequence

IC218LZr. Alloy IC218LZr solidifies by initial formation of $\gamma$ dendrites which subsequently precipitate $\gamma'$ cubes. The remaining liquid freezes in a "starburst" $\gamma$-$\gamma'$ eutectic reaction. Figure 2 schematically describes the solidification sequence with the corresponding microstructure. The composition of phases, as determined by EDS analysis, is presented in Table II. Qualitatively, these results agree well with those previously published for similar alloys.[6]

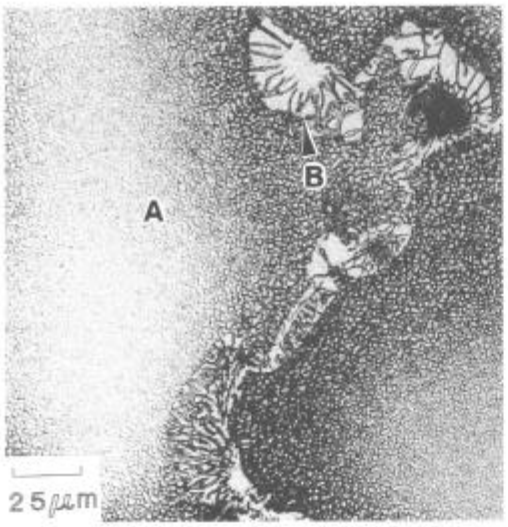


(a)

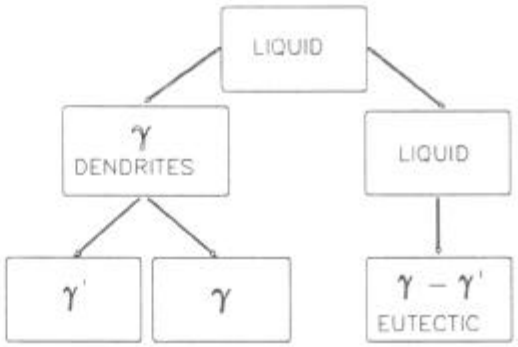


(b)

**Figure 2.** IC218LZr: (a) As-cast structure: (A) Dendrite, (B) Starburst; Kalling's etch. (b) Schematic solidification sequence.

Table I. Nominal Compositions of IC221 and IC218LZr

| | Weight % | | Atomic % | |
|---|---|---|---|---|
| Element | IC218LZr | IC221 | IC218LZr | IC221 |
| Al | 8.7 | 8.5 | 17.0 | 16.7 |
| Cr | 8.1 | 7.8 | 8.2 | 8.0 |
| Zr | 0.2 | 1.7 | 0.1 | 1.0 |
| B | 0.02 | 0.02 | 0.1 | 0.1 |
| Ni | Bal | Bal | 74.6 | 74.2 |

Table II. Composition of Phases in As-Cast IC218LZr as Determined by EDX Analysis (Refer to Figure 2).

| Area | Composition Weight % | | | |
|---|---|---|---|---|
| | Al | Cr | Ni | Zr |
| Dendrite (A): | | | | |
| Cube (γ') | 10.2 | 7.1 | 82.5 | 0.2 |
| Intercube (γ) | 7.2 | 8.6 | 84.2 | 0 |
| Starburst (B): | | | | |
| Cell (γ') | 10.0 | 6.0 | 82.8 | 1.2 |
| Intercell (γ) | 7.2 | 10.2 | 82.2 | 0.4 |

IC221. Alloy IC221 initially solidifies by the same sequences as IC218LZr, as seen in the schematic in Figure 3. However, due to the higher zirconium content, a lower melting point eutectic completes the solidification. The resulting interdendritic structure consists of a Zr-rich phase which co-precipitates with γ rods. The γ rods appear as a dendritic

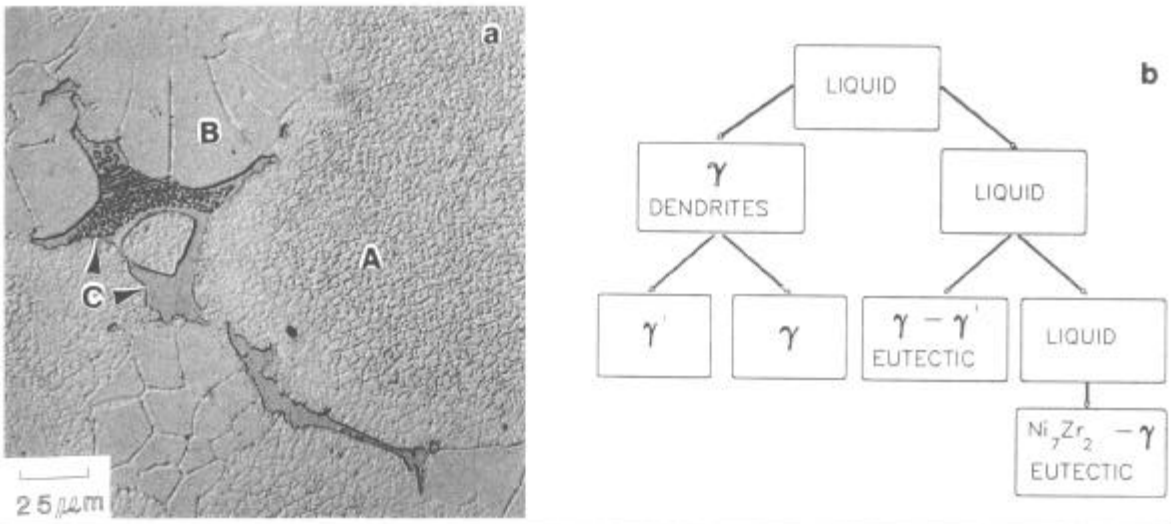


**Figure 3.** IC221: (a) As-cast structure: (A) Dendrite, (B) Starburst, (C) Eutectic; (Electrolytic etch.) (b) Schematic of solidification sequence.

or dot pattern on metallographic samples (Figure 3a). It was discovered that the Zr-rich phase will etch heavily and leave cavities if aggressive etchants such as Kalling's are used. (Note when comparing the metallographic structures of Figures 2 and 3 that different etchants were used.) To preserve the Zr-rich phase in IC221 and reveal the structure, a mild electrolytic etch was applied (20% sulphuric acid in methanol, 16 V for 30 sec). This technique dissolves the $\gamma$ phase at a slightly higher rate, leaving a gentle contrast. The IC218LZr was etched in Kalling's, which results in the $\gamma'$ phase appearing white. The composition of the various phases in IC221 is summarized in Table III. The general compositional trends for the $\gamma$ and $\gamma'$ phases are the same as for IC218LZr. However, the composition of the Zr-rich phase appears to correspond to the intermetallic phase $Ni_7Zr_2$ by the atomic ratio of Ni to Zr detected (Ni/Zr = 3.4). Similar phases have previously been identified as $Ni_5Zr$[6-8], which is consistent with the Ni-Zr binary phase diagram.[9] However, both quantitative EDX analysis at Special Metals and WDX analysis at the University of British Columbia indicate a composition corresponding to $Ni_7Zr_2$. The reason $Ni_7Zr_2$ forms rather than $Ni_5Zr$ is not fully understood. We speculate that it is due to the strong attraction of nickel to aluminium, which will decrease the activity of nickel in solution, in combination with the strong segregation of zirconium to the interdendritic liquid.

Finally, the $\beta$ phase was not detected in either IC218LZr or IC221 contrary to what has previously been suggested for similar alloys.[6]

## Microstructure After Heat Treatment

The effects of elevated temperature exposure were evaluated by differential thermal analysis (DTA) and gradient bar heat treatment of alloy IC221. The DTA curve for IC221 (Figure 4) exhibits two distinct and one weak endothermic reactions. The first reaction, which initiates at 1146 °C and peaks at 1172 °C, is consistent with an incipient melting reaction. This reaction is clearly associated with the zirconium-containing phase, since the DTA curve for IC218LZr does not exhibit this peak as seen in Figure 5. The second, less well-defined reaction which initiates at approximately 1200 °C, appears to be the result of solutionizing of a broad range of $\gamma'$ structures. These two reactions probably overlap somewhat. The third reaction is a classical melting reaction with solidus and liquidus temperatures of 1300 °C and 1362 °C, respectively. The phase reactions observed by DTA were verified by metallographic evaluation of a gradient bar

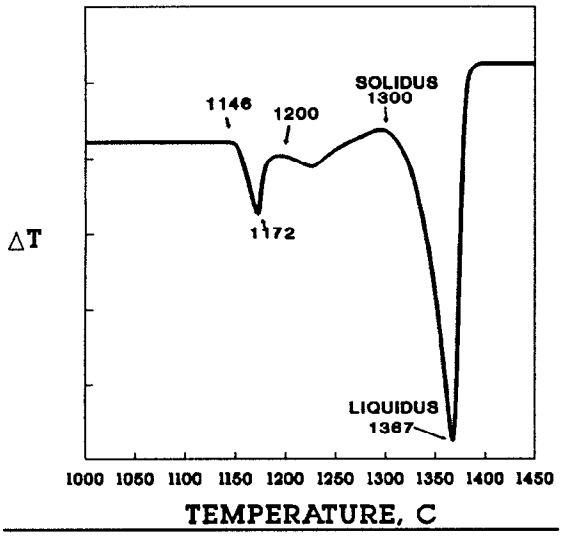


Figure 4. DTA curve for alloy IC221. Heating rate: 10°C/min.

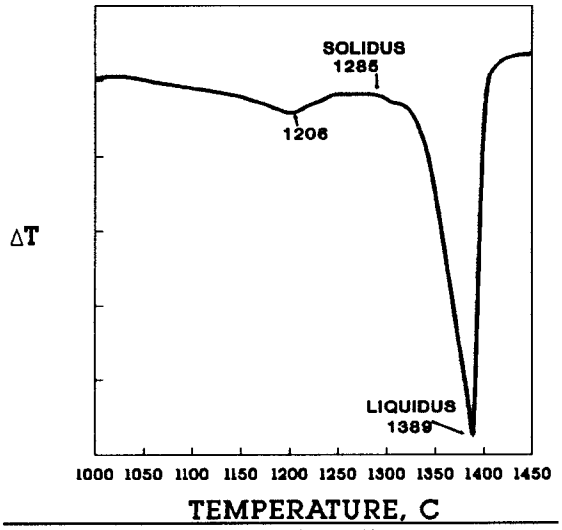


Figure 5.DTA curve for alloy IC218LZr. Heating rate: 10°C/min.

treated for twelve hours at 871°C to 1204°C. The structure exhibits only small changes up to 1100°C; the $\gamma'$ precipitates coarsen and the amount of $Ni_7Zr_2$ appears to decrease, as seen in Figure 6. At 1121°C, the $Ni_7Zr_2$ phase has clearly started to solution and is almost completely eliminated at 1149°C. At 1149°C, the first traces of incipient melting can also be detected, identifying the distinct reaction with a DTA peak at 1172°C as an incipient melting reaction. At 1204°C the incipient melting reaction is more obvious, as is the further solutioning of $\gamma'$. Thus, three reactions are obvious from the gradient bar, but only two peaks are present on the DTA diagram. The results indicate that the undetected reaction is the solutioning of $Ni_7Zr_2$, already complete at 1150°C. This reaction is probably too slow and has too low a heat of reaction to be detected by the DTA technique. To further confirm our hypothesis, samples were isothermally heat treated at 1180°C and 1250°C followed by water quenching. At 1180°C, areas of incipient melting are present, as seen in Figure 7; at 1250°C, only minute traces of $\gamma'$ can be detected. This confirms that the DTA peak at 1172°C corresponds to the incipient melting reaction of the Zr-rich eutectic and that the shallower peak at 1243°C corresponds to the solutioning of $\gamma'$.

## Mechanical Properties

Tensile Properties. As-cast ingots were evaluated in the temperature range of 760 to 1040°C at a strain rate of 0.06/min, and samples from the 406 mm IC221 ingot were also tested at a strain rate of 0.005/min. Transverse tensile samples from the 406 mm IC221 ingot were taken from a slice cut from near the top of the ingot and longitudinal test bars were taken from an adjacent slice. Transverse tensile samples from the 102mm IC221 and IC218LZr ingots were taken from slices cut from near the top of the ingots.

Figure 8 shows 0.2% yield strength versus temperature for IC218LZr and IC221. The results indicate that the yield strength of IC221 in the temperature range of 750 to 1000°C is consistently 40 to 70 MPa higher than that of IC218LZr. The IC221 curve closely agrees with results published by Sikka[4] on cast tubes. Duplicate samples of IC221 (i.e. one sample from each size ingot) tested at 815°C, 871°C and 982°C produced essentially identical results. The duplicate samples tested at 760°C did, however, show a decrease in yield strength of about 50 MPa for the 406 mm ingot. This is presumably the result of the slightly coarser grain structure of the 406 mm ingot as compared to the 102 mm ingot. Previous work[4] indicates that the tensile strength of IC221 is fairly sensitive to microstructure at temperatures below 800°C and relatively insensitive at temperatures at or above 800°C. The tensile results also indicate that the ductility of IC221 at temperatures of 750°C to 1000°C is approximately 15% better than the

Table III. Composition of Phases in IC221 as Determined by EDX and WDX Analysis (Refer to Figure 3)

| Area | Composition [weight %] Al | Cr | Ni | Zr |
|---|---|---|---|---|
| Dendrite (A): | | | | |
| Cube ($\gamma'$) | 8.6 | 7.9 | 83.3 | 0.2 |
| Intercube ($\gamma$) | 6.0 | 9.2 | 84.5 | 0.3 |
| Starburst (B): | | | | |
| Cell ($\gamma'$) | 8.5 | 6.6 | 81.9 | 3.0 |
| Intercell ($\gamma$) | 5.1 | 10.8 | 83.4 | 0.7 |
| Eutectic (C): | | | | |
| Zr-rich phase | 0.5 | 1.2 | 67.4 | 30.9 |
| Rods | 6.0 | 12.2 | 79.7 | 2.1 |

ductility of IC218LZr, as seen in Figure 9. These results are not unreasonable, as we are comparing the as-cast properties of an alloy designed for wrought applications (IC218LZr) with those of an alloy designed for casting. The effect of strain rate on the yield strength of IC221 is presented in Figure 10. At temperatures above 850°C, an increase in strain rate from 0.005/min to 0.06/min results in an increase in strength of approximately 100 MPa. However, samples tested at 760°C and 815°C did not exhibit any shift in strength. This abrupt change in strain rate sensitivity appears to be the result of the shift in the predominate deformation mechanism from lattice slip to grain boundary slip. Grain boundary slip is a shear process occurring in the direction of the grain boundary, which is promoted by increasing the temperature and/or decreasing the strain rate.[10]

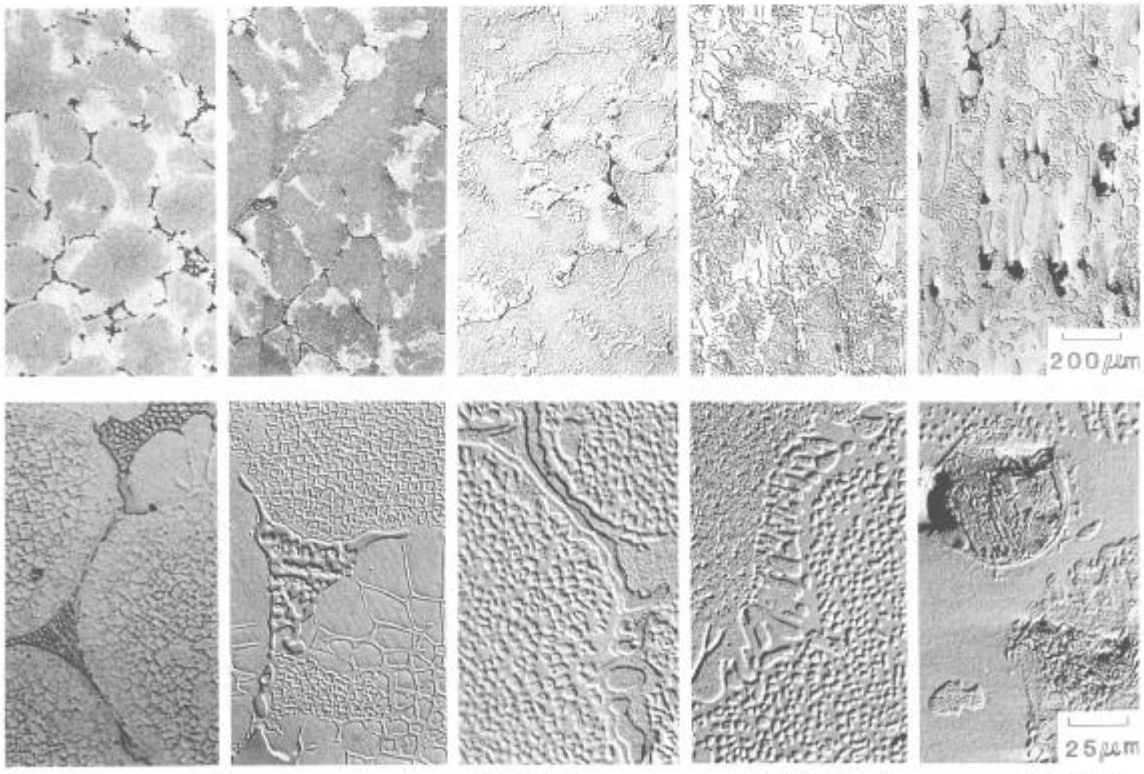


**Figure 6.** Microstructure of IC221 gradient bar treated for 12 hours and water quenched. Temperatures as indicated.

Compression Testing. The 406 mm IC221 ingot was tested in the temperature range between 760°C and 1040°C to evaluate compressive strength' and between 1093°C and 1177°C to evaluate hot workability and structural refinement. Longitudinal test bars measuring 10.2 mm in diameter by 15.2 mm in height, and test bars measuring 38.1mm in diameter by 76 mm in height were cut from the top of the ingot. The 38.1 mm samples were isothermally pressed to 50% of their original height at a constant engineering strain rate of 0.5/min.

Figure 11 is a plot of the 5% offset yield strength for IC221. IN718 data has been added for comparison. In the temperature range tested, IC221 exhibits approximately a 300 MPa advantage in compressive strength over IN718.

Figure 12 presents photographs of the as-tested surface and the longitudinal macrostructure of samples tested in the temperature range of 1093°C and 1177°C. All samples exhibit severe intergranular cracking which increases with temperature. The macrostructures of the lower temperature tests also exhibit improved grain refinement compared to the samples tested at higher temperatures. Based on this analysis, two additional samples were isothermally pressed under the following conditions:

| | | | |
|---|---|---|---|
| Sample 1: | upset 23% at 1093°C<br>H.T. 1135°C-18 Hrs-AC<br>upset 66% at 1038°C | Sample 2: | upset 33% at 1093°C<br>H.T. 1135°C-18 Hrs-AC<br>upset 63% at 1038°C |

The workability of both samples was greatly improved. Sample 2 contained some light cracks, presumably due to the initial upset. Both samples exhibited a relatively fine structure with the exception of the top and bottom die lock areas. The cross-sectioned macrostructure and general surface condition of sample 1 is presented in figure 13.

Hardness of Gradient Heat Treated Bars

Two bars from the 406 mm diameter IC221 ingot were gradient heat treated at 815°C to 1260°C for four and twelve hours, respectively, followed by water quenching. A third bar of IC221 and a bar of IC218LZr were heat treated at 1149°C for four hours, water quenched, then gradient heat treated at 760°C to 1093°C for twelve hours and water quenched. After preparation, the internal hardness of the bars was evaluated at room temperature. The results are presented in Figures 14 and 15.

The increase in hardness from 930°C to 1200°C for the gradient heat treated bars is attributed to the solutioning of $\gamma'$. It appears that the increase in hardness results from

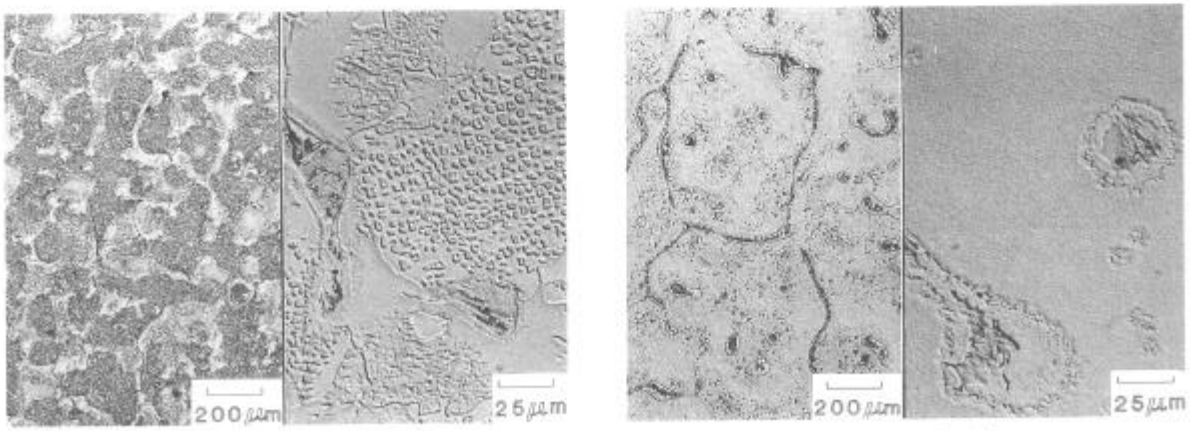


1180 C; 2h 1250 C; 2h

Figure 7. Microstructure of isothermally treated and water quenched samples of IC221.

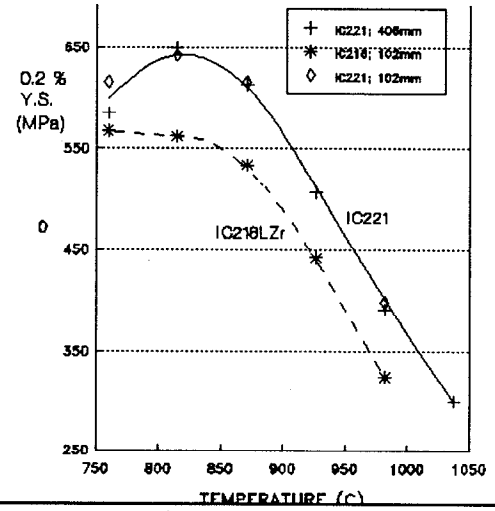


Figure 8. Elevated temperature yield strength of alloys IC221 and IC218LZr.

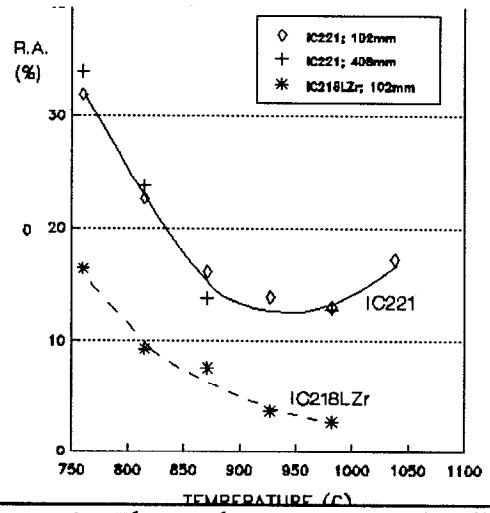


Figure 9. Elevated temperature ductility of alloys IC221 and IC218LZr.

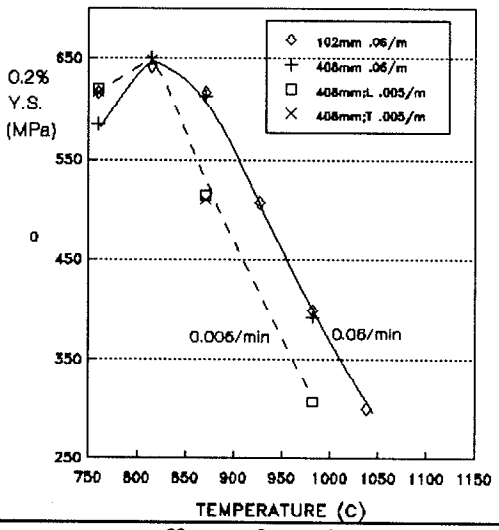


Figure 10. Effect of strain rate on the yield strength of alloy IC221.

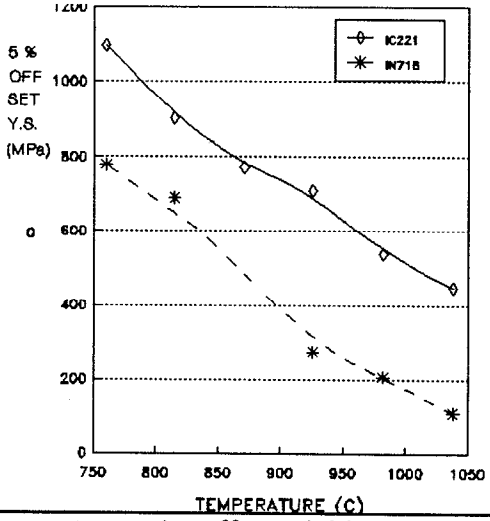


Figure 11. 5% offset yield strength of IC221.

a combination of solid solution hardening and the precipitation of fine cooling $\gamma'$ on quenching. The lower hardness of the bar treated for 12 hours could be due either to additional annealing of the matrix or to differences in the initial structure of the bars.

Although the hardness of IC221 and IC218LZr is significantly different as seen in Figure 15, (results for IC221 are given in Rc and results for IC218LZr in Ra) the shapes of the curves are similar, suggesting the same hardening mechanisms. At 1149 C considerable amounts of $\gamma'$ are solutioned while the lower temperatures coarsen existing $\gamma'$ resulting in reduced hardness. The minimum hardness is obtained when all $\gamma'$ is reprecipitated and overaged. Further reduction in temperature reduces the rate of $\gamma'$ coarsening resulting in higher hardness due to aging.

## Summary Discussion

This investigation indicates that production- scale $Ni_3Al$-base alloy ingots can be produced without unmanageable segregation or ingot cracking. Mechanical test results show that, in spite of severe segregation of zirconium, as-cast IC221 exhibits both better

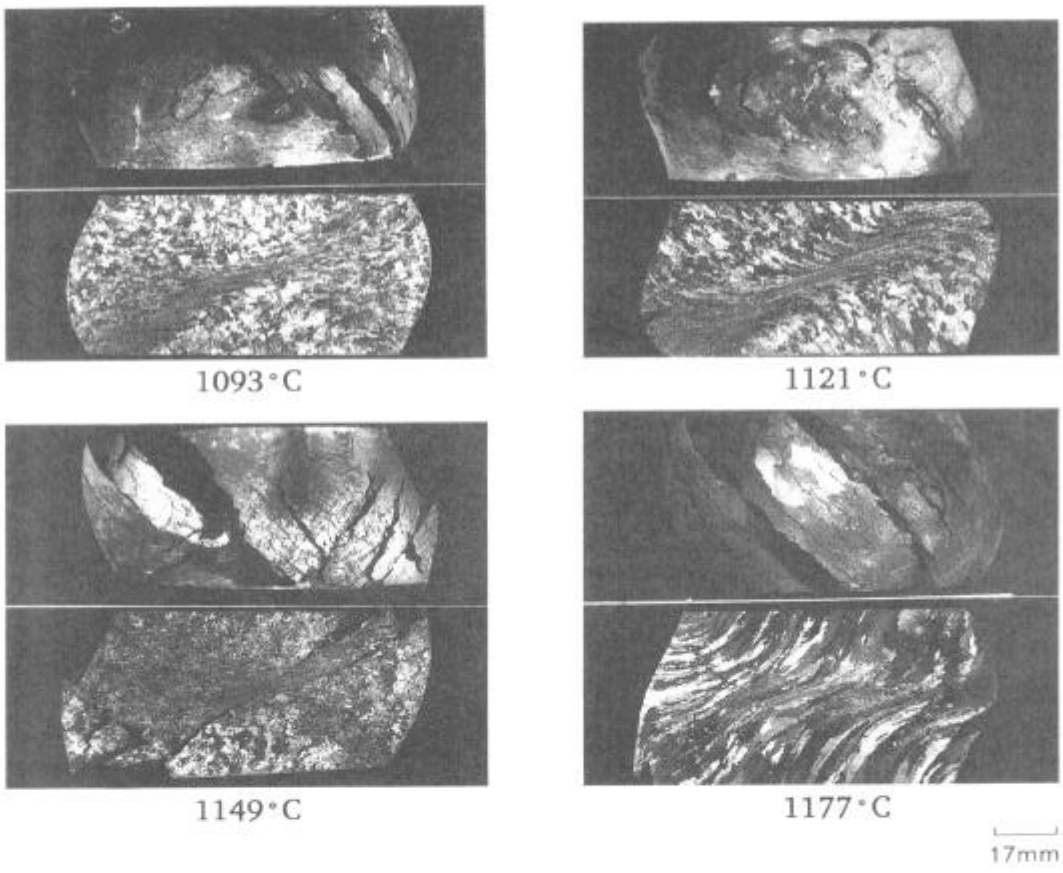


Figure 12. As-tested surfaces and longitudinal macrostructures of samples isothermally upset at temperatures indicated.

strength and ductility than as-cast IC218LZr, as well as better compressive strength than IN718 at temperatures from 750°C to 1000°C. Heat treating results indicate that the alloys can be homogenized and that the room temperature mechanical properties can be changed through heat treatment. Additional development is needed to fully understand and utilize the heat treatment responses.

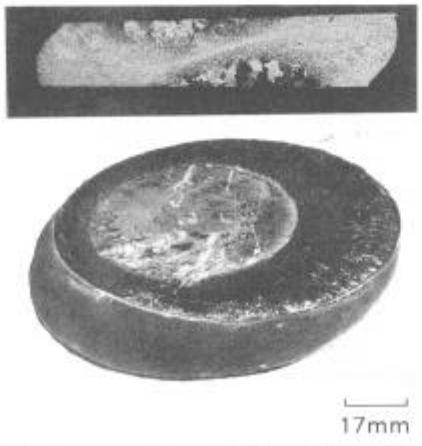


Figure 13. As-tested surface and longitudinal macrostructure of Sample 1.

From a fundamental point of view, the results obtained show the presence of $Ni_7Zr_2$ in IC221 rather than $Ni_5Zr$, as would be expected from the binary phase diagram. While the reason for the formation of $Ni_7Zr_2$ is not fully understood, we speculate that it is due to the strong attraction of nickel to aluminium which leads to reduced nickel activity in combination with heavy segregation of zirconium to the interdendritic fluid.

Acknowledgements

The support of the personnel of Ladish and SMC in producing and evaluating the material, as well as in preparing the manuscript is gratefully acknowledged. We also thank Alec Mitchell and Al Schmaltz of the University of British Columbia for their assistance with WDX analysis and technical discussions.

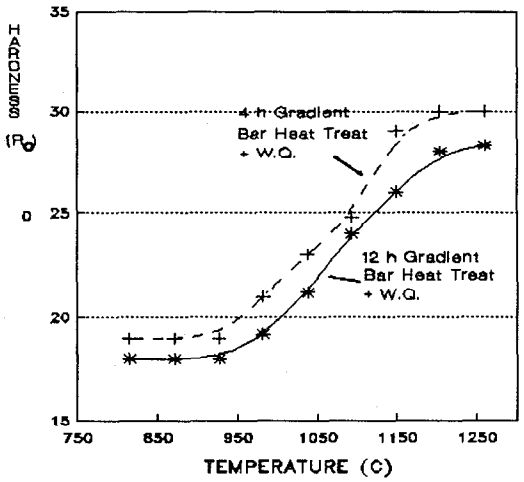


Figure 14. Room temperature hardness of gradient bars.

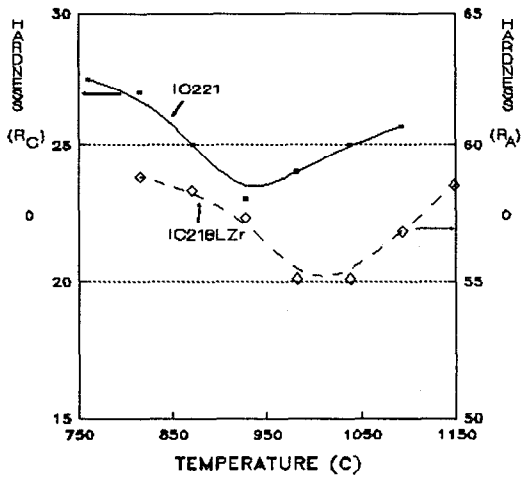


Figure 15. Room temperature hardness of bars 1149°C-4-WQ + gradient heat treatment.

References

1. N. S. Stoloff, "Physical and Mechanical Metallurgy of $Ni_3Al$," International Metallurgical Review, 34 (4) (1989), 153-183.

2. D. P. Pope and C. T. Liu, "Strength and Ductility of Intermetallic Compounds," Superalloys, Supercomposites, and Superceramics, (Academic Press, 1989) 583-624.

3. S. Sen and D. M. Stefanescu, "Melting and Casting Processes for High-Temperature Intermetallics, JOM, May, 1991, 30-34.

4. V. K. Sikka and E. A. Loria, "Industrial Scale Processing and Elevated Temperature Properties of $Ni_3Al$-Cr-Zr-B Alloys," Superalloys 1988, (Warrendale, PA: The Metallurgical Society, 1988), 203-212.

5. V. K. Sikka, "Commercialization of Nickel Aluminides," High Temperature Aluminides and Intermetallics, TMS 1989, 505-520. Symposium on High Temperature Alumindes and Intermetallics.

6. C. T. Ho, C. J. Cheng, and J. A. Sekhar, "Solidification Microporosity in Directionally Solidified Multicomponent Nickel Aluminide," Metallurgical Transactions A, 22A (1991), 225-234.

7. Z. Yunrong, W. Yuping, Z. Jizhon, P. Caron, and T. Khan, "Effect of Chemistry Modifications and Heat Treatments on the Mechanical Properties of DS MAR-M200 Superalloy," Superalloys 1988, (Warrendale, PA: The Metallurgical Society, 1988), 335-344.

8. T. H. Chuang and Y. C. Pan, "On The Mechanisms of High-Temperature Intergranular Embrittlements of $Ni_3Al$-Zr Alloys," Metallurgical Transactions A, 23A (1992), 1187-1193.

9. P. Nash and C. S. Jayanth, "The Ni-Zr System," Bulletin Alloys Phase Diagrams, 5 (2) (1984), 144-148.

10. G. E. Dieter, "Mechanical Metallurgy," (McGraw-Hill, Inc. 1976), 460T